Spring 2024

Optical Fiber Magnetic Field Detector

Aiden Tomov , '24

Paige Poteet , '24

Optical Fiber Magnetic Field Detector

ENGR 090:
Senior Design Project

by

Aiden Tomov[*] & **Paige Poteet**[†]

Supervised by Professor Lynne Molter

May 16, 2024

[*]Email: atomov1@swarthmore.edu
[†]Email: ppoteet1@swarthmore.edu

Abstract

This project demonstrates an optical approach to magnetic field detection. Operating as an adapted Mach-Zender interferometer, the apparatus begins by splitting an infrared beam of light into two separate paths, each with 50% of the overall power. These paths are segments of single-mode photonic crystal fiber (PCF) and are of equal lengths. One of the PCF paths has its air holes infused with EMG 700 ferrofluid which, by nature of ferrofluids, has a tunable refractive index (RI). The beams are recombined and shone into a power meter for analysis. When the ferrofluid-infused path encounters a magnetic field, the RI within the fiber changes due to the presence of EMG 700, thereby causing a change in the effective travel distance for the mode of light. Thus, when the beams reunite, there will be interference. Depending on the strength of the magnetic field, the magnitude of the interference will change accordingly, resulting in a detectable relationship between the power of the emergent light and magnetic field strength.

Table of Contents

1 Introduction **1**

2 Theory **2**

2.1 Refractive Index Changes with Ferrofluid 2

2.2 Propagation Delay vs Index of Refraction 4

2.2.1 Deriving Propagation Delay Model 4

2.2.2 Modeling the Propagation Delay in a PCF 5

3 Methods **6**

3.1 Design Specifications 7

4 Results **9**

4.1 Theoretical Results 9

4.2 Experimental Results 13

5 Discussion and Conclusion **15**

6 Future Work **16**

Appendices **17**

A Sam's Michelson Interferometer **17**

B Acknowledgments **17**

C MATLAB code for 2.1 **17**

D MATLAB code for 2.2 **19**

References **21**

1 Introduction

Detecting magnetic fields is necessary for many institutional practices, and the advancement of this capacity is critical to preserving human health and security. In medicine, identifying irregularities in the weak magnetic pulses generated by neural activity can alert doctors to various neurological disorders. Similarly, the recognition of the action currents which generate magnetic fields in the heart warns of heartbeat irregularities and murmurs. In fields of industry, the stability of mines and the functionality of equipment is ensured through magnetic field detection. Even in the military, sensing the relative strength of a magnetic field with an acute sensitivity is essential to detecting stealth aircrafts and warships.

As a broadly important tool, it is unfortunate that the latest technologies for magnetic field detection are expensive and bulky. Furthermore, many in-lab magnetometers rely on the Hall effect which, as a simple RC circuit, is prone to electromagnetic interferences. Such a weakness is a concern for scientists working in labs with a range of electronic devices or those in industry seeking compact sensors that provide reliable magnetic field data. This project aims to create a fiber optical system capable of responding to relatively small changes in magnetic field strength. The benefit of an optical apparatus is the sensitivity, speed, and processing power at which light operates. Furthermore, photonic technology is scalable, with the potential to be reduced to an on-chip component. While the system that we are proposing is considerably spacious and fragile, a proof of concept would pave the way for a more elegant implementation of our sensor in the following couple of years.

Our design is an adapted Mach-Zender interferometer with two arms of Photonic Crystal Fiber (PCF). The interference occurs due to RI changes of the ferrofluid infused into one of the fiber arms. Our lab is equipped with the materials and theoretical background to realize this design. In the Swarthmore Optics Lab, we have a substantial history in interferometry and fiber optical sensors. One of the lab's collaborators, Sam Goldwasser, developed a Michelson interferometer apparatus that motivated the use of interferometry in our design and has given us extensive practice in the alignment procedure. Additionally, our lab has completed several fiber optic systems for different purposes in the past, most notably a fiber bending sensor and a fiber twisting sensor. Thus, we have the equipment and ability to work with emergent interference patterns from our system.

2 Theory

The Mach-Zender Interferometer is a precision instrument that produces interference fringes by splitting a light beam into two parts and then recombining them after they have traveled different optical paths. In general, interferometers are highly sensitive to differences (in lengths, RI, etc.) in their arms. Any distinction between the arms that causes interference at even a fraction of the wavelength causes noticeable results, which are measured with a detector such as a power meter.

Our adaptation splits our light source into two PCFs with equal power in each. The light within a fiber propagates through the core which is at a higher index of refraction than the surrounding cladding. Depending on the cladding's refractive index, the light will bounce at oblique angles corresponding to the RI. By changing the cladding's RI, the effective distance the light travels in the fiber can change, creating an exploitable source of interference.

2.1 Refractive Index Changes with Ferrofluid

In this section, we present derivations introduced by [1], and [2]. Our work synthesizes and explains these equations in the context of our research.

The RI changes of ferrofluid as a function of magnetic field was initially described by [1]. The group injected Fe_3O_4, a water based ferrofluid, into a thin cell and covered it with a silicon triangular prism. This prism serves as a polarizing maintaining (PM) interface for light to travel through. An incident beam of infrared was illuminated through the prism, upon the ferrofluid-infused cell, and back out to a detector. The detector scanned the intensity of the beam at various angles of incidence. The results yield the following expression for the RI of ferrofluid:

$$n_{MF} = \frac{1}{2}(\sqrt{2n_p^2 - 2\sin^2\theta_{it}} - \sqrt{2}\sin\theta_{it}) \tag{2.1}$$

Where n_{MF} is the refractive index of the ferrofluid, n_p is the refractive index of the prism, and θ_{it} is the angle of incidence of the beam on the PM interface that allows total reflection. From here, further work is needed to determine an intrinsic energy dependence.

We note that two critical, physical energies align ferrofluid particles via exposure to magnetic fields. These are the magnetic energy and the thermal energy of particles in the field. The basis for understanding this relationship lies within the fundamental principles of paramagnetism. The term paramagnetism describes elements that possess a permanently magnetized moment, such as ferrofluid's constituent particles. Masses of ferromagnetic particles do not self-align because their magnetic moment's are too weak, instead sitting in a pool with their moments oriented at random. However, upon facing an induced field, this mass of ferromagnetic particles align with their moments facing the same vector-direction as the magnetic field.

We describe the alignment of these ferroparticles mathematically with a specific form of the Langevin function. The Langevin function is an energy-balance function for quantum

systems. It works within the inherent confines of the uncertainties within small-scale systems' energies. It is of the form,

$$L(x) = coth(x) - \frac{1}{x} \tag{2.2}$$

We can begin by formulating a Langevin function with a derivation of the probability of the energy interactions of some ferrous particles with a specific energy, E, given by $E = -\hat{\mu} * \hat{B}$, where $\hat{\mu}$ is the magnetic dipole moment. The probabilistic derivation is achieved with a Boltzmann statistic:

$$\rho_{Bol} = e^{-E/(k_B T)} = e^{\mu B \cos\theta/(k_B T)} \tag{2.3}$$

Where k_B is the Boltzman constant, and θ is the angle between the moment and the induced field. The direction of the moment is susceptible to change, not its magnitude. This is due to the intrinsic properties of the ferromagnetic particles. A particle with a vector that represents its magnetic moment can move such that it's vector may point in any direction. Thus, it forms an imaginary sphere with magnitude r around itself. The probability that the moment aligns by some $d\theta$ in relation to the induced magnetic field is derived as,

$$\rho(\theta, T, B) = \frac{e^{\mu B \cos\theta/(k_B T)} \sin\theta}{\int_0^\pi e^{\mu B \cos\theta/(k_B T)} \sin\theta d\theta} \tag{2.4}$$

With this, we obtain an expression for the magnetization of the ferromagnetic particles per unit volume as,

$$M = \int N\mu \cos\theta \rho(\theta, T, B) = N\mu \frac{\int_0^\pi e^{\mu B \cos\theta/(k_B T)} \cos\theta \sin\theta d\theta}{\int_0^\pi e^{\mu B \cos\theta/(k_B T)} \sin\theta d\theta} \tag{2.5}$$

Here, N is an expression for the amount of moments per volume. Solving the integrals and simplifying the solution, we obtain is,

$$M = N\mu \left[\coth(\frac{\mu B}{k_B T}) - \frac{k_B T}{\mu B} \right] \tag{2.6}$$

We see that Eq. 2.6 is in the form of our Langevin function, Eq. 2.2, where $x = \frac{\mu B}{k_B T}$.

This returns us to our adapted Langevin equation. We modify Eq. 2.6 to a generalized form for a thin ferrofluid film. The expression adapts the magnetization of the ferrous particles to, specifically, the fluid's refractive index. We obtain,

$$n_{MF}(H, T) = [n_s - n_o] * \left[\coth(\alpha \frac{H - H_{c,n}}{T}) - \frac{T}{\alpha(H - H_{c,n})} \right] + n_o \tag{2.7}$$

We see the proportionality term, $[n_s - n_o]$ where n_s is the saturated value of the fluid's refractive index, and n_o is the refractive index of the fluid before it reaches $H_{c,n}$, the magnetic

field strength in which the refractive index begins to change. Additionally, we have α as our model's fitting parameter. We also note that we change our parameters from B to H because we are no longer concerned with an intrinsic magnetic property, B, but an induced, changing field, H.

This model is fit to [3]'s data. The result supports their experimentally found, approximately linear change in ferrofluid's refractive indices within an operating range inherent to the fluids. Beyond this range the magnetic field becomes too intense and begins to damage the composition of the fluid.

The work done in this paper will explore the parameters of this model. Developing a model specific to the ferrofluid used in our design, EMG 700, we can determine a threshold of magnetic field values that the fluid is sensitive to for the testing of our magnetometer.

2.2 Propagation Delay vs Index of Refraction

Propagation delay in the fiber is described as the time duration taken for the light to cross the fiber of length z.

2.2.1 Deriving Propagation Delay Model

The model that will be referenced for this section is created by the works of Meenakshi and Ravichandran[4].

The variation of wavelength due to the refractive index can be expressed as a modified Sellmeir formula

$$n = c_0 + c_1\lambda^2 + c_2\lambda^3 + \frac{c_3}{(\lambda^2 - 0.035)} + \frac{c^4}{(\lambda^2 - 0.035)^2} + \frac{c_3}{(\lambda^2 - 0.035)^3} \tag{x}$$

The wavelength, λ, is in units of microns. The wavelength itself ranges from $(\lambda_m - \frac{\sigma}{2})$ to $(\lambda_m + \frac{\sigma}{2})$, where λ_m is considered the source center wavelength (which is also known as the the peak emitted wavelength of any source), and σ is the spectral width of the source. In respect to this model, the source will be set as a beam of light emitted from a laser and each laser has a specified wavelength. The c_i variables present in (x) are constant coefficients that vary depending on the material, in the case of a PCF the material is pure Silica.

The propagation delay function, $\tau(\lambda, m')$ is given by,

$$\tau(\lambda, m') = \frac{zN_1}{c}\left[1 + \frac{(\alpha - 2 - \xi)}{(\alpha + 2)}\Delta(m')^{\frac{\alpha}{\alpha+2}} + \frac{(3\alpha - 2 - 2\xi)}{2(\alpha + 2)}\Delta^2(m')^{\frac{2\alpha}{\alpha+2}}\right] \tag{2.8}$$

where, z is the length of the fiber, N_1 is the group index, and ξ is the correction factor which is dependent on the wavelength of the source. N_1 and ξ are given by,

$$N_1 = n_1 - \lambda \frac{\partial n_1}{\partial \lambda} \tag{2.8a}$$

and

$$\xi = \frac{-2n_1\lambda}{N_1\Delta}\frac{\partial \Delta}{\partial \lambda} \tag{2.8b}$$

The optimum value of α is dependent on the doping material used for variations in the refractive index. Doping material creates impurities in fiber core or cladding which is typically pure Silica. Dopants such as GeO_2 or Al_2O_3 are typically used in order to create a high-refractive-index core and the low-refractive index cladding. Assuming that the impure doping material or no doping material is equally dispersed across the core of the fiber, the optimum value and α is given by,

$$\alpha = 2 - \epsilon\Delta + \xi \tag{2.9}$$

where ϵ is a constant that ranges from $0 < \epsilon < 4$.

2.2.2 Modeling the Propagation Delay in a PCF

To model the propagation delay in a Photonic Crystal Fiber (PCF) which dependence on the refractive index of the cladding, the propogation delay function, $\tau(\lambda, m')$, given in **Eq. 6** will be altered to become dependent on refractive index. The propagation delay function was analyzed in order to find how the refractive index of the cladding relates to the propagation delay. τ is the variable for the propagation delay given in units of seconds, λ is the wavelength that is moving through the core of the fiber given in meters, and m' equivalent to $\frac{m}{M}$ where m is the mode of the fiber and M is the highest mode the fiber can support. The variable m' was set to a constant of 1 which can be interpreted as having a fiber that can support a single mode, in this case the PCF that is being modeled can filter out other modes which will be interpreted as the fiber being able to support one mode, and the propagation of the light will also only be single mode. After setting m' to a constant, λ is also set to a constant. The refractive index of the cladding will now become the dependent term and the function will be new propagation delay function is given by,

$$\tau(n_2) = \frac{zN_1}{c}\left[1 + \frac{(\alpha - 2 - \xi)}{(\alpha + 2)}\Delta(m')^{\frac{\alpha}{\alpha+2}} + \frac{(3\alpha - 2 - 2\xi)}{2(\alpha + 2)}\Delta^2(m')^{\frac{2\alpha}{\alpha+2}}\right] \tag{2.10}$$

The variable z is the length of the fiber which ultimately can change the time of the propagation delay directly since a longer fiber will increase propagation delay and a shorter fiber will decrease the propagation delay. The variable c is the speed of light, this is an important factor since light itself is being propagated to the fiber and $c = 3 * 10^8 m/s$.
To find the refractive index of the core, (x) is used and the coefficients c_i have values that were experimentally determined given a specified material. The material of the core is pure Silica, so the given coefficients are: $c_0 = 1.4508554$ $c_1 = -0.0031268$ $c_2 = -0.0000381$

$c_3 = 00.0030270$ $c_4 = -0.0000779$ $c_5 = 0.0000018$.
The α value is dependent on the impurity of the fiber, for this model the PCF will be entirely pure Silica which and contain no impurities which will set $\alpha = 2 - 2\Delta + \xi$.

3 Methods

A schematic for our apparatus is shown below with a corresponding reference key. Note that the design is fixed to a TMC vibration control laboratory tabletop.

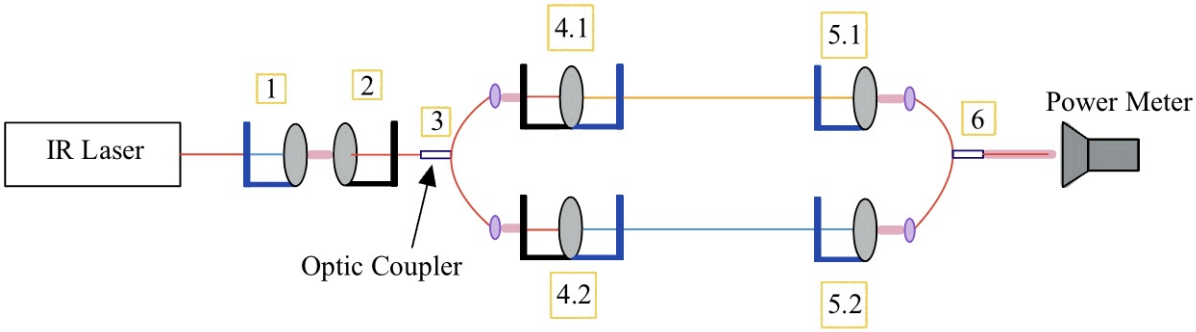

Figure 1: Magnetic Interference labeled Schematic

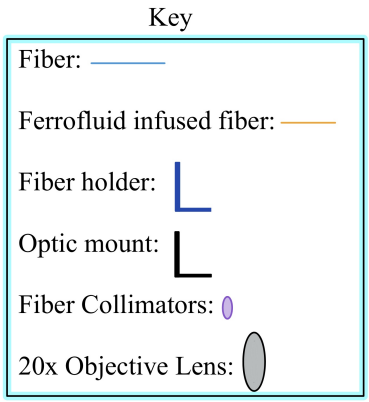

Figure 2: Components Key for Schematic

To begin the setup shown in Figure 1, we obtained an infrared (IR) *G&H* high power, DFB laser, pigtailed to a single core fiber. The fiber is fixed to a mount and shone into a 20x lens that is used to collimate the light, labeled at point 1 in Figure 1.

At each point in the diagram, the mounts must be adjusted and aligned using micrometers to ensure precise coupling of the beam into the ensuing fiber or lens. This is necessary to ensure the minimization of power loss through each component. Typically, our IR laser was set to operate at $50mA$ which yields $3.1mW$ of power. Each objective lens results in the loss of $\approx 20\%$ of the overall power. This means, for example, that at point 1, the power is already attenuated to $2.5mW$. Precise alignment is critical to attaining results from the design.

After collimation, the beam at point 1, the light is refocused into a ThorLabs TN1550 fiber optic coupler, which splits the light into two paths of equal power. The ends of these couplers are fitted with collimating lenses and refocused at points 4.1 and 4.2 into a foot of single mode PCF. The cross section of the PCF is shown below:

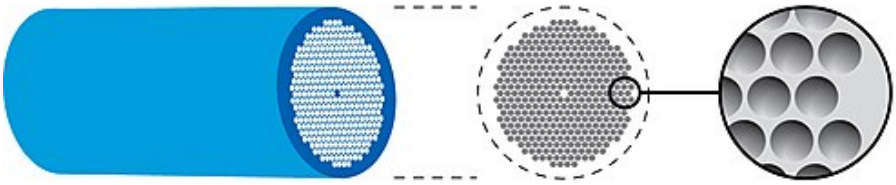

Figure 3: Cross Section of Photonic Crystal Fiber

As seen in Figure 3, the core of the PCF is surrounded by airholes. In the upper path, from point 4.1 to 5.1, the airholes are infused with Ferrotec's EMG 700 ferrofluid. At points 5.1 and 5.2, the beams emerge from the PCF and are focused into another TN1550 coupler where they recombine.

After the paths recombine at point 6 in the coupler, the resultant beam exits and is incident on a Coherent power meter. Here, we collect our data for analysis.

Returning to the ferrofluid-infused path of PCF between points 4.1 and 5.1, we have a permanent magnet attached to a linear stage, stationed beneath it. Here, the adjustment of the distance from the magnet to the fiber allows us to manipulate the refractive index of the ferrofluid. Changes in the RI causes the effective distance traveled by the light propagating through the PCF to increase and decrease. The subtle changes in path length traveled are the basis of the interference in our apparatus: As the beams recombine at point 6, the interference creates power differences that we analyze with our power meter.

The propagation delay in the PCF depends on the refractive index of the cladding. Since the PCF's cladding in on of the arms contains ferrofluid, the refractive index of the cladding is approximately equivalent to the refractive index of the ferrofluid. The propagation delay function, $\tau(n1)$, given in **Eq. 2.10**. To determine the experimental propagation delay, the propagation delay function is plotted against various refractive indices through MATLAB. The laser that is used had a wavelength of $\lambda = 1550nm$ which is also known as far infrared. This wavelength will be a constant used in this model as well as the length of the fiber which was cut to be approximately $0.381m$.

3.1 Design Specifications

Currently, there are no Engineering standards regarding the detection of magnetic fields using optical fibers. The design goal of this project is to identify the presence or absence of a magnetic field generated by a large permanent magnet. Because our method is novel, optimization of our design to increase its sensitivity and ability to measure the intensity of

the magnetic field can be pursued later. This may only be done after we have validated our ability to detect a magnetic field reliably. Thus, the design specification for this project is to detect a magnetic field with a signal strong enough to be statistically distinguishable from noise.

4 Results

4.1 Theoretical Results

To test the strength of the two permanent magnets, a Lake Shore 455 DSP Gaussmeter was obtained. The strength of the magnet was tested at various distances which resulted in the following graphs below.

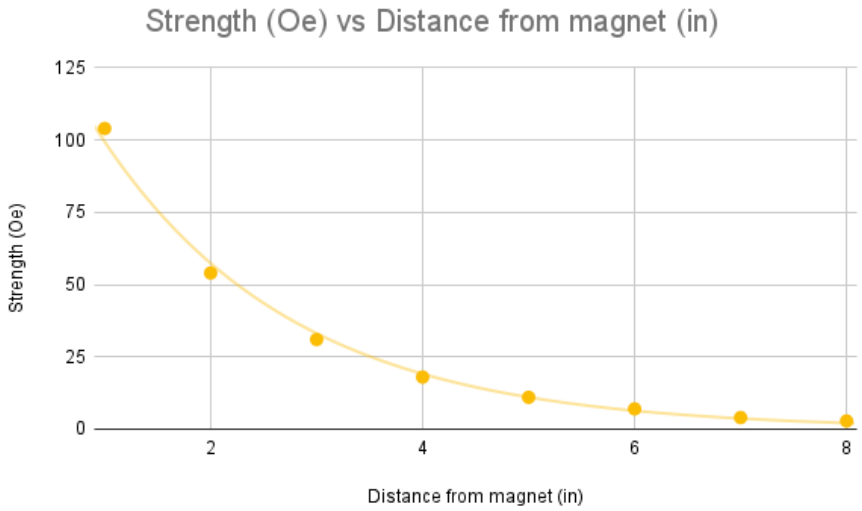

Figure 4: Weak Magnet's Strength as a Function of Distance

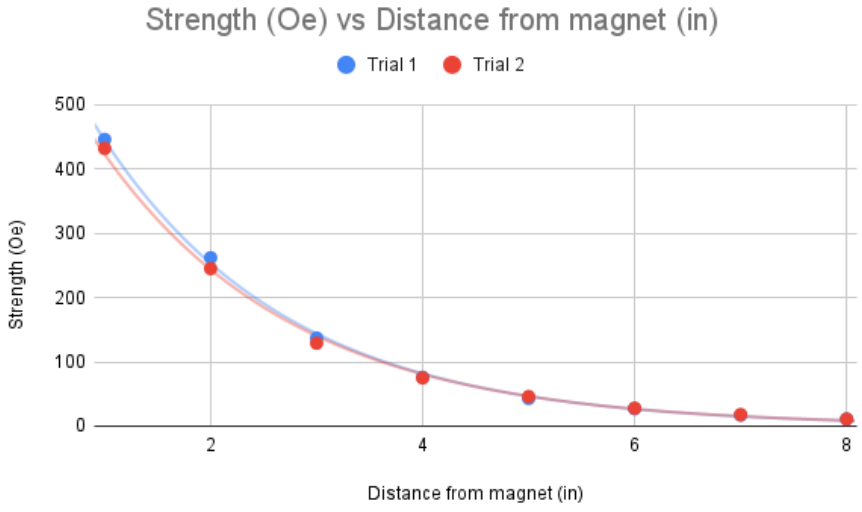

Figure 5: Strong Magnet's Strength as a Function of Distance

Knowledge of the field strength allows us to test our design with a known intensity by simply manipulating the distance of the magnet to the fluid-infused fiber. Furthermore, knowing

that, within a critical operating range, the RI of the ferrofluid changes at an approximately linear rate, allows us to map our magnetic field intensity to refractive index change.

The model for RI change in ferrofluid is shown in Equation 2.7 to be:

$$n_{MF}(H,T) = [n_s - n_o] * \left[\coth(\alpha\frac{H - H_{c,n}}{T}) - \frac{T}{\alpha(H - H_{c,n})}\right] + n_o \tag{4.1}$$

Our lab contacted the research and development team at Ferrotec who provided estimates for the parameters in our RI model. According to Ferrotec, the typical refractive index of their ferrofluid, EMG 700, is around 1.420. Thus, we can determine $n_o = 1.420$. They also expressed that a typical range for magnetic field intensity allowing RI modulation is 0–700 Oe. Linear modulation of the RI begins at around 25 Oe. Therefore, we can determine H_c = 25 Oe.

Furthermore, according to [1], the change in refractive index within the linear region of change is $\pm 5 \times 10^{-3}$, so we can estimate our value of n_s to be around 1.425. Our laboratory at Swarthmore has an average temperature of 70°F or 294.3K. In the following measurements, we will at first treat temperature as constant, then study how our results change with fluctuating temperature.

Without knowledge of the true fitting parameter, α, for our ferrofluid, our approach was to understand, in general, how the RI changes at various values of α. Below is a plot of RI versus magnetic field for several fitting parameter values.

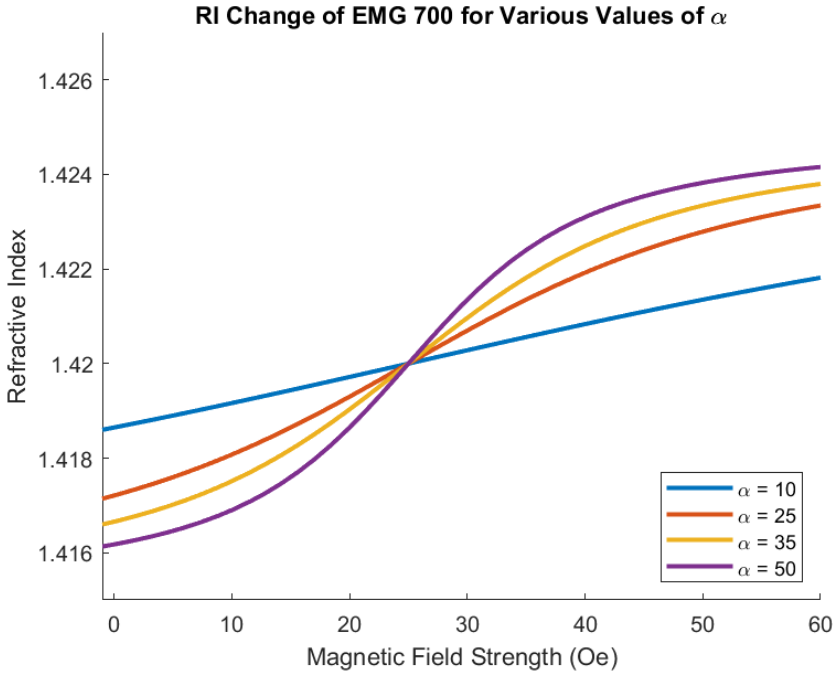

Figure 6: RI Change for Various Values of α

Next, we averaged theoretical results over a range of typical α values. These fitting parameters span from $1 - 50$. The resulting model is shown below:

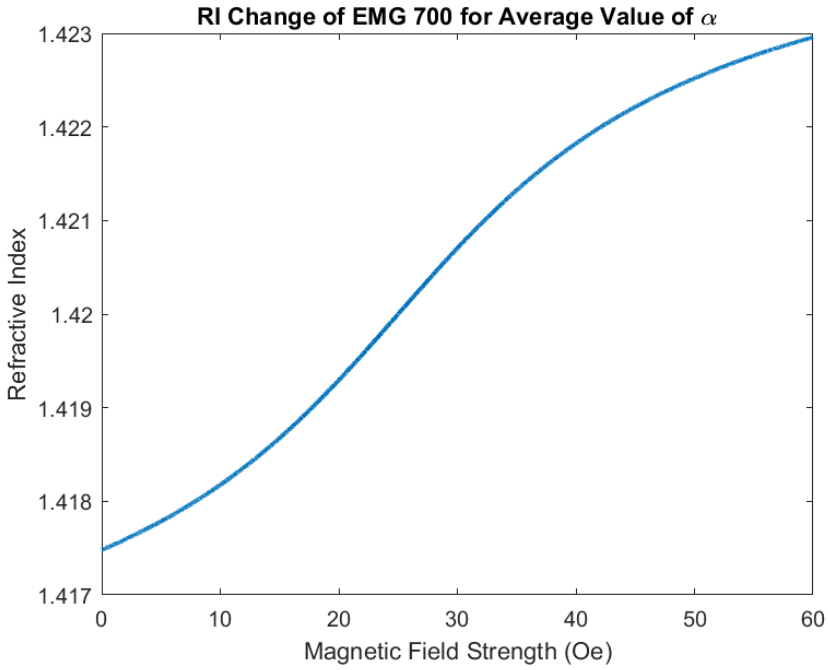

Figure 7: RI Change Averaged Over α = 1-50

A first-degree polynomial is fit to Figure 7 to determine an estimate for the changes in the RI within this model over an average α. The fit is shown here:

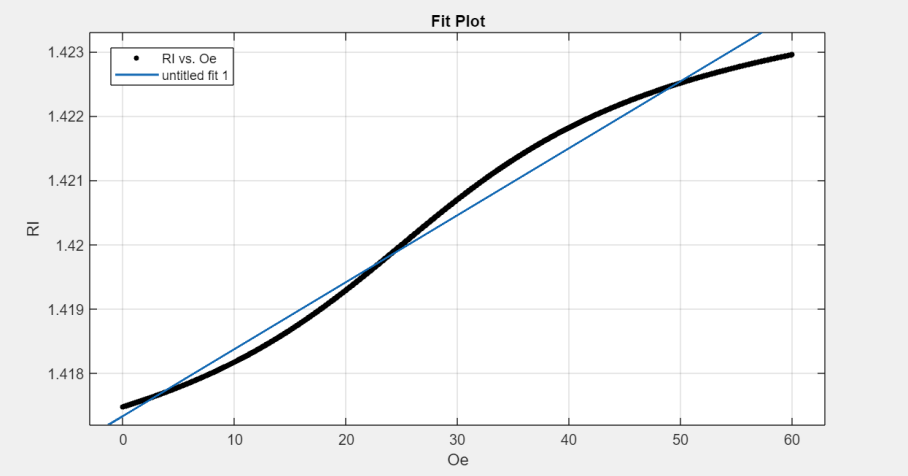

Figure 8: First-Degree Polynomial Curve Fit

The equation for the curve-fitted expression is $y = 1.042 \times 10^{-4}x + 1.417$ with an R-Square value of 0.9827 and an RMSE of 2.395×10^{-4}. This indicates a strong fit and supports the

assumption that this region of the RI change can be reasonably modeled as linear. For our team at Swarthmore College's optics lab, without knowing a specific α value for the EMG 700, being able to reasonably predict a linear change between 0 and 60 Oe is affirming for our work.

A final consideration for the RI model is temperature fluctuations. In our lab, the temperature is 70°F, though, according to the college, fluctuations can range from $68° - 76°$F. This corresponds to a range of $293 - 298$K. The RI change was modeled for the lower and upper bounds temperatures as well as the average temperature of 70°F.

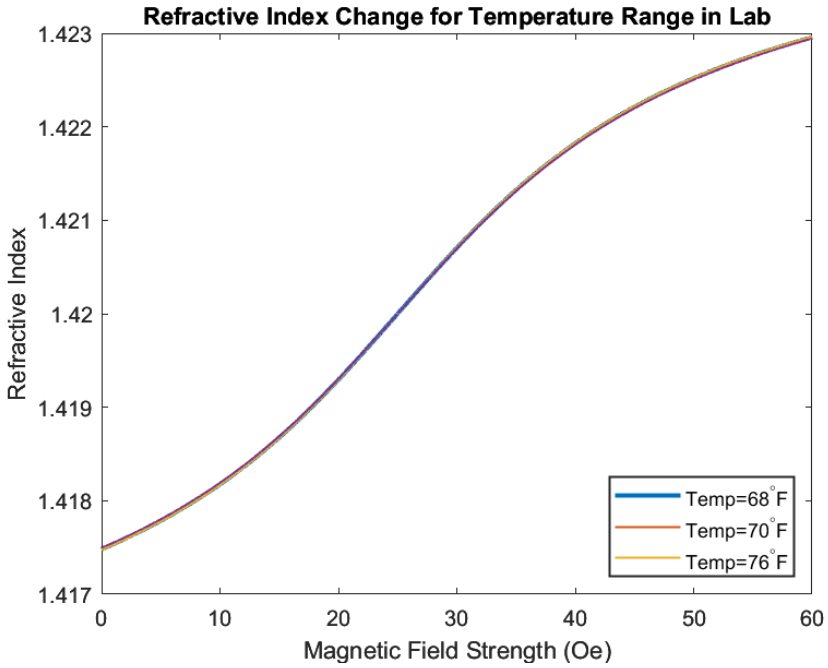

Figure 9: RI Change for Upper and Lower Bound Temperatures

Visually, the difference between these curves is minimal. The first-degree polynomial curve fits support this assessment. The plot of the lower bound temperature, 68°F is fitted to the equation of $y = 1.044 \times 10^{-4}x + 1.417$ with an R-square of 0.9826 and an RMSE of 0.0002411. The plot of the upper bound temperature, 76°F is fitted to the equation $y = 1.034 \times 10^{-4}x + 1.417$ with an R-square of 0.9831 and an RMSE of 0.0002348.

The difference in slope of the fitted expression between the average temperature for the lab versus the upper and lower bound values is between 0.0000002 and 0.0000008. The range in values for the slope are 1.034×10^{-4} and 1.044×10^{-4}. This means there is a maximum difference of 0.768% in the slope of these fitted equations.

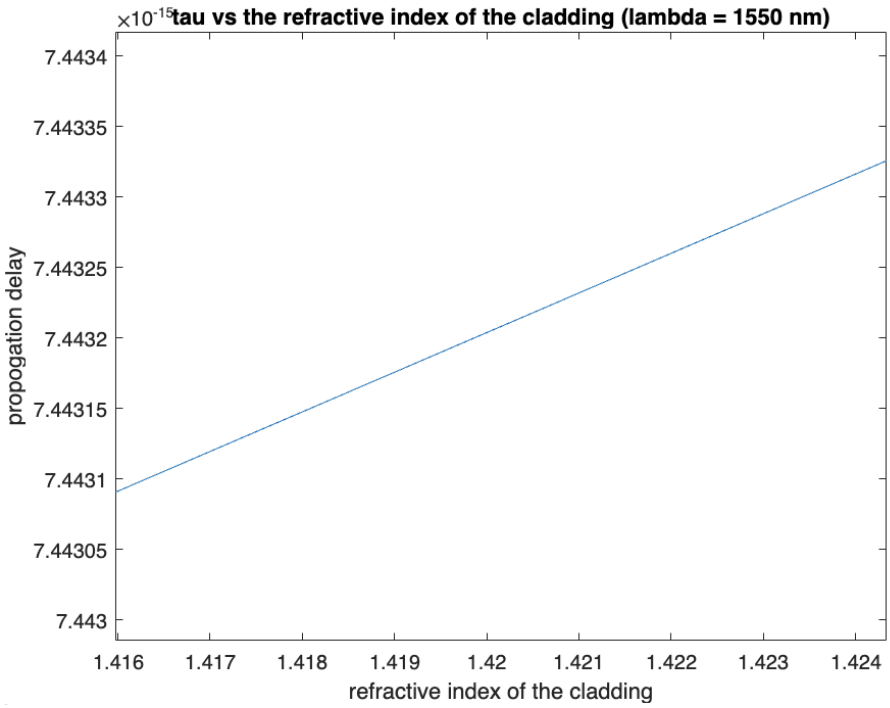

Figure 10: RI Change Averaged Over α 1-50

The RI of the EMG 700 is known to range from approximately (1.416,1.424) when it is in the presence of a magnetic field. The propagation delay is then affected within these changes as seen in **Fig. 8**. The linear relationship proves that any small changes in the RI will drastically be shown through the interferemoter. Although this does not give an accurate depiction of what the output values would look like from a power meter, it gives insight into how drastic we can assume the output to be. Any small changes in the propagation delay will be amplified through the interference.

4.2 Experimental Results

Upon recombination of the two beams and without the presence of a magnetic field, our device records an average power reading of around $50nW$ when the laser operates at $75mA$. Additionally, we observed that the recombined beam, without any magnetic field, is unstable. This could indicate system instability in our device, potentially from vibrations or fluctuations of power contributed from the laser. The optical coupler used to recombine the beams may also possess an intrinsic defect.

Despite these fluctuations, the presence of a magnetic field increases the power out of the device. In the presence of a $45Oe$ magnetic field, the power doubles. In the presence of the magnetic field, instability in the system remains a factor. This is likely due to the same vibration or power fluctuation issues, plus a delay of the RI shift in the ferrofluid.

Furthermore, these results are repeatable and consistent between various power inputs to the

device. This supports the legitimacy of the system by accounting for an erroneous test or series of tests.

5 Discussion and Conclusion

The outcomes of this research have provided a novel alternative to traditional magnetic field detection without the disadvantage of inaccurate readings due to electromagnetic interference. However, there remain challenges that we faced throughout this process and in the interpretation of our results.

Before analyzing the experimental results, the theoretical results are crucial to understanding the system's response to the magnetic field. The magnetic field causes minute changes in the RI of the cladding which, in turn, changes the propagation delay linearly. The small changes in the propagation delay cause changes in the overall interference that we observed through the power meter. Using the theoretical values, it is possible to map the interference to the changes caused by the magnetic fluid within a range of values in which the RI of that fluid changes to a first-order, linear approximation. Unfortunately, due to time constraints, the analysis portion is not yet completed. But, through understanding the theory, this will be completed in future work with our design.

Throughout the design process, there were some limitations that were discovered during the setup of our apparatus. Primarily, power loss posed a significant issue, especially during the initial stages of the setup. We found that the lenses in our lab created, approximately, 21% of power loss whereas optical couplers accounted for, approximately, 20% of power loss. To minimize the amount of loss experienced, two lenses were replaced with fiber collimators, which result in no power loss. These fiber collimators attach themselves to the end of the couplers, eliminating the need to align those specific components. Secondly, due to time constraints, the alignment of our current model is not currently set up to maximize the amount of power going through the apparatus.

Despite these limitations, this design has proven to reliably detect magnetic fields. With more time for experimentation and alignment, the current apparatus will have the sensitivity to detect weaker magnetic fields, and the data from the device will be mapped to a specific magnetic field intensity.

6 Future Work

Future iterations of this project will highlight two main improvements. The first is the union of the junctions in the setup. The main difficulty in setting up the design is the transmission of power between elements. By connectorizing the various elements to allow for seamless transitions, we can minimize the power loss. Currently, we lose 99.9% of the power from the laser through our system. Thus, not only is our current setup energy inefficient, but it is also relying on weak signals for data extraction.

Moreover, the lack of direct connections is the most likely source of power fluctuation in our design output. The noise in the data limits our ability to dictate the precise magnetic field intensity values as well as the sensitivity of the sensor. By creating ideal junctions in our design, we can reduce the power lost in element transitions and smooth our data.

Finally, our design will be tested for specific power readings in relation to specific magnetic field values. This will be done through measurements and corroboration with a gaussmeter. We can support these experimental results theoretically by measuring the value of the propagation delay given a magnetic field reading.

Appendices

A Sam's Michelson Interferometer

B Acknowledgments

We would like to thank Sam Goldwasser who helped us with Michelson Interferometry, J Johnson for building essential components that we used in our final design, and Cassy Burnett for organizing and arranging delivery of our project's components. We also would like to issue a very special thank you to our advisor and mentor Professor Lynne Molter who provided advise and limitless support throughout the completion of this project.

C MATLAB code for 2.1

```
% Code for Mathematical Modeling (Math 56) Project
% We want to model the refractive index of ferro-
% fluid as a function of the magnetic field inten-
% sity of the surrounding magnetic field.
% We also want to inspect how the temperature flux
% in our lab may influence our results
clear
% Define our variables
n_s=1.425;   % saturated value of fluid's RI
n_o=1.420;   % critical RI (before change)
H_c=25;    % critical H (point where RI begins change)
Temp=294.3;    % approx lab temperature
alpha=50;

% Simulate values for H
syms H

RI50=(n_s-n_o)*(coth(alpha*[H-H_c]/Temp)-(Temp)/(alpha*[H-H_c]))+n_o;

alpha=10;
RI10=(n_s-n_o)*(coth(alpha*[H-H_c]/Temp)-(Temp)/(alpha*[H-H_c]))+n_o;

alpha=25;
RI25=(n_s-n_o)*(coth(alpha*[H-H_c]/Temp)-(Temp)/(alpha*[H-H_c]))+n_o;

alpha=35;
RI35=(n_s-n_o)*(coth(alpha*[H-H_c]/Temp)-(Temp)/(alpha*[H-H_c]))+n_o;




hold on
fplot(RI10, 'LineWidth', 2)
fplot(RI25, 'LineWidth', 2)
fplot(RI35, 'LineWidth', 2)
fplot(RI50, 'LineWidth', 2)
axis([-1 60 1.415 1.427]);
```

```
title("RI Change of EMG 700 for Various Values of \alpha")
legend("\alpha = 10","\alpha = 25","\alpha = 35","\alpha = 50",'location', 'southeast')
xlabel("Magnetic Field Strength (Oe)")
ylabel("Refractive Index")
hold off
```

```
alpha=50;

x=zeros(601);
for i=1:length(x)
    x(i)=(i-1)*.1;
end

RI=zeros(601);
for h=1:length(x)
    RI(h)=(n_s-n_o)*(coth(alpha*[x(h)-H_c]/Temp)-(Temp)/(alpha*[x(h)-H_c]))+n_o;
end

plot(x,RI)
axis([-1 60 1.415 1.427]);

cftool
```

```
Oe=zeros(6001, 1);
for i=1:length(Oe)
    Oe(i)=(i-1)*0.01;
end
RI=zeros(6001, 1);
for alpha=1:50
    for h=1:length(Oe)
        RI(h)=RI(h)+((n_s-n_o)*(coth(alpha*[Oe(h)-H_c]/Temp)-(Temp)/(alpha*[Oe(h)-H_c]))+n_o);
    end
end
RI=RI/50;
```

```
plot(Oe,RI, 'LineWidth', 2)
title("RI Change of EMG 700 for Average Value of \alpha")
xlabel("Magnetic Field Strength (Oe)")
ylabel("Refractive Index")

cftool
```

```
Temp=293

Oe293=zeros(6001, 1);
for i=1:length(Oe293)
    Oe293(i)=(i-1)*0.01;
end
RI293=zeros(6001, 1);
for alpha=1:50
    for h=1:length(Oe293)
        RI293(h)=RI293(h)+((n_s-n_o)*(coth(alpha*[Oe293(h)-H_c]/Temp)-(Temp)/(alpha*[Oe293(h)-H_c]))+n_o);
    end
end
RI293=RI293/50;

Temp=298

Oe298=zeros(6001, 1);
for i=1:length(Oe298)
    Oe298(i)=(i-1)*0.01;
end
RI298=zeros(6001, 1);
for alpha=1:50
    for h=1:length(Oe298)
        RI298(h)=RI298(h)+((n_s-n_o)*(coth(alpha*[Oe298(h)-H_c]/Temp)-(Temp)/(alpha*[Oe298(h)-H_c]))+n_o);
    end
end
RI298=RI298/50;

hold on
```

```
plot(Oe, RI, 'linewidth', 1)
plot(Oe293, RI293, 'linewidth', 1)
plot(Oe298, RI298, 'linewidth', 1)
title("Refractive Index Change for Temperature Range in Lab")
legend("Temp=68^{\circ}F", "Temp=70^{\circ}F", "Temp=76^{\circ}F", 'location', 'southeast', 'linewidth', 1)
hold off

cftool
```

D MATLAB code for 2.2

```
%Plotting the Propogation delay as a function of the index of refraction and the
%mode of the fiber
clear
syms x
%tau = propogation delay
%lamda = wavelength
%m = mode of the fiber
%M = highest mode the fiber can support
%tau(lambda,m/M)
%z = length of the fiber


%tau(lambda,m/M) = z*N/c*[1-(alpha-2-xi)/(alpha+2)*delta*
% (m/M)^(alpha/(alpha+2))+(3*alpha-2-2*xi)/(2*alpha+4)*
% delta^2(m/M)^(2*alpha/(alpha+2))]
%x = lambda;
%y = tau
l_list = [.8*10^(-6),.8*10^(-6),.85*10^(-6)];
%for i=1:3
%The fiber will be a single mode fiber that can support two modes depending
%on the wave length, so
m = 1;
M = 1;
%the length of the fiber is 15 in which
z = 0.381;
% c = speed of light (rounded) m/s
c = 3*10^8;

%Cn are coefficients given for Silica material
C0 = 1.4508554;
C1 = -0.0031268;
C2 = -0.0000381;
C3 = 00.0030270;
C4 = -0.0000779;
C5 = 0.0000018;

%set lambda to x so derivative can be taken n1 = refractive index of core
n1 = C0 +C1*x^2 + C2*x^4 + C3/(x^2-0.035) + C4/(x^2-0.035)^2 + C5/(x^2-0.035)^3;

dn = diff(n1);

%N = correction factor depending on wavelength
N = n1-x*dn;
xi = -2*n1*x/N;
%n2 = refractive index of cladding
n2 = 1;
delta = (n1^2-n2^2)/(2*n1^2);
ddelta = diff(delta);
xi = (-2*n1*x)/(N*delta)*ddelta;
%optimum alpha value is given below (eq7a)
alpha = 2-2*delta+xi;
lambda = x;
lambda = 1.55*10^(-6);
n2 = x;
power = alpha/(alpha+2);
p1 = (alpha-2-xi)/(alpha+2)*delta*(m/M)^power;
p2 = (3*alpha-2-2*xi)/(2*(alpha+2))*delta^2*(m/M)^(2*power);
y = (lambda*N/c)*(1+p1+p2);


```

```
hold on
fplot(x,y)
title('Propagation Delay vs RI')
xlim([-2,2]);
%ylim([6*10^(-15),7.6*10^(-15)]);
xlabel('Refractive Index of the Cladding')
ylabel('Propogation Delay (s)')
%legend({'1550 nm','1200 nm','850 nm'})
%end

```

References

[1] Shieh-Yueh Yang, Yu-Te Chen, Herng-Er Horng, Chin Yih Hong, W. S. Tse, and H. C. Yang. Magnetically-modulated refractive index of magnetic fluid films. *Applied Physics Letters*, 81:4931–4933, 2002.

[2] Shand. Physics of modern materials. *Magnetic Materials, University of Northern Iowa*, pages – Lecture Notes 1–12, 2024.

[3] Chin-Yih Hong, H. E. Horng, and S. Y. Yang. Tunable refractive index of magnetic fluids and its applications. *physica status solidi (c)*, 1(7):1604–1609, 2004.

[4] M. Meenakshi and V.C Ravichandran. Wavelength dependent $\alpha - profilemodelofmultimodefiber - opticchannel$, 1998.